Tunable mantle cloaking utilizing graphene metasurface for terahertz sensing applications

Research Article | Vol. 27, No. 24 / 25 November 2019 / Optics Express 34824

Optics EXPRESS

Tunable mantle cloaking utilizing graphene metasurface for terahertz sensing applications

ZAHRA HAMZAVI-ZARGHANI,[1,2] ALIREZA YAHAGHI,[1,4] LADISLAU MATEKOVITS,[2] AND ALI FARMANI[3,5]

[1] School of Electrical and Computer Engineering, Shiraz University, Shiraz 71946, Iran
[2] Dipartimento di Elettronica e Telecomunicazioni, Politecnico di Torino, 10129, Torino TO, Italy
[3] School of Electrical and Computer Engineering, Lorestan University, Iran
[4] yahaghi@shirazu.ac.ir
[5] farmani.a@lu.ac.ir

Abstract: Design of sensors which are able to probe electromagnetic radiation with larger cross section and at the same time with having negligible perturbation in measurement has attracted significant attention. For this purpose, scattering-cancellation sensors or cloaking sensors are introduced. However, tunable cloaking sensors are very challenging. In this regards, here, a metasurface based on graphene strips is proposed to cloak a dielectric cylinder under illumination of TE_z and TM_z polarized incident waves in terahertz range. According to the in plane effective surface impedance tensor for the considered metasurface and the required surface impedance for achieving invisibility under *TE* and *TM* polarized impinging waves, the geometrical parameters of the covering structure and characteristics of graphene are obtained. Numerical simulations show radar cross section reduction for both *TE* and *TM* polarizations. Furthermore, the introduced metasurface is able to cloak the cylinder for incoming waves with circular polarization. In addition, it is shown that by properly adjusting the chemical potential of graphene, the required surface impedance to have cloaking for the two polarizations in other frequencies can also be achieved, which results in a tunable dual polarized cloaking. The proposed structure provides 2-11 dB reduction in scattering strength relative to the uncloaked configuration for 0.3eV variation of graphene chemical potential.

1. Introduction

Cloaking techniques have been demonstrated to lead to highly effective tools that are able to sense electromagnetic radiation, especially at terahertz frequencies with negligible perturbation [1–13]. Different approaches have been proposed for cloaking purpose such as transformation optics [14,15] plasmonic cloaking [16,17] and so on [18–22]. Mantle cloaking is one of the most effective methods showing notable performance and comfortable realization [23,24]. Since in a mantle cloak, the object is covered by a thin metasurface, the proposed cloaking devices have low profile and weight and good flexibility to be formed in a desired shape [25, 26]. At microwave frequencies, patterned metallic sheets have been used as the covering metasurface to achieve the required surface impedance aimed at cancelling the scattered field of the object by producing an anti-phase scattered wave [27,28].

In this regards, several invaluable studies have been presented in literature to make dielectric and conducting cylinders invisible especially for TM_z polarized incident wave propagating in the x direction, i.e, orthogonal incidence. As an example Matekovits et al. [29], considered cloaking of multiple dielectric cylinders. Covering the cylinders by width-modulated microstrip line based mantle cloak has significantly reduced their scattering. Also, Teperik et al. [30], experimentally reported ultra-thin metasurface cloak for hiding a metallic obstacle. In their work, radar cross section (RCS) of conducting cylinders has been remarkably suppressed by coating them with patterned metallic surfaces. Some researches have been devoted to increase cloaking bandwidth.

#375836 https://doi.org/10.1364/OE.27.034824
Journal © 2019 Received 20 Aug 2019; revised 31 Oct 2019; accepted 31 Oct 2019; published 13 Nov 2019

Optics EXPRESS

For instance in Granpayeh research group [31,32], metasurfaces based on disks with different sizes have been utilized to cover dielectric cylinders and spheres, respectively in order to create resonances in different frequencies leading to a broad bandwidth. Therefore, metasurfaces have been received remarkable attention from research groups [33–35]. However, noble metasurfaces have relatively high ohmic loss and tunability of their optical properties are challenging [36–39].

To solve the above issue graphene is introduced in [40–46]. Graphene, a two dimensional material, as a allotropes of carbon has attracted significant attention because of its extraordinary properties such as strong light-matter interaction, low ohmic loss, and transparency [47–51]. One of the most important characteristics of graphene is its electrical and optical tunability which results in designing various tunable and reconfigurable devices in electronics and photonics realm [52–55] such as: switches and logic gates [56–58], reconfigurable lenses [59,60], tunable polarization converters [61,62] and tunable absorbers [63,64] and some other applications [65–71]. Tunable mantle cloaking can also be achieved with graphene monolayers or patterned graphene metasurfaces. In [72], scattering of a dielectric cylinder under illumination of TM_z polarized oblique incidence has been reduced using a graphene monolayer. Graphene monolayer is inductive in terahertz range and therefore can not cloak conducting cylinders which needs capacitive surface impedances [73]. To cope with this issue, a nanostructured graphene metasurface with negative reactance has covered a conducting cylinder in order to make it invisible [48]. In the both cases, frequency of cloaking has been tuned by changing the chemical potential of graphene [74]. The majority of researches related to cloaking have been done with consideration of TM_z polarized impinging wave propagating in the x direction. This is because this incident wave produce more pronounced scattered fields compared to *TE* polarized impinging wave [75]. However, the scattered field from a TE_z illuminated wave is not negligible and in some applications it is necessary to cloak a cylinder under illumination of a TE_z polarized wave. Dual polarized mantle cloak can be a good choice to reduce scattering from a cylinder for both *TE* and *TM* polarizations. To achieve mantle cloaking for *TE* and *TM* polarizations, an anisotropic metasurface should be designed. With an anisotropic metasurface, one can independently control the surface impedance in each direction, leading to achieve the required values of it for both polarizations in a given frequency [76]. We propose graphene strips as a covering metasurface whose surface impedance tensor has been derived in [77]. In [76], dual polarized cloaking has been achieved in a fixed frequency. However, in our proposed structure, the frequency of dual polarized cloaking can be tuned by adjusting the chemical potential of graphene. This is the highlight feature of the proposed structure.

The rest of this paper is organized as follows. In Section II, the optical and geometrical properties of the proposed sensor is presented and studied. In the same section, the metasurface to achieve the considered goal is designed. Then, in Section III, cloaking behaviour of the structure is investigated. Therefore, numerical results of RCS for uncloaked and cloaked cylinders are illustrated proving scattering reduction for *TE*, *TM* and circular polarizations. In the same section, the tunable optical properties are considered and cloaking responses further extracted through numerical simulation. Then, in Section IV, finally, we summarize the main conclusions.

2. Designing an anisotropic metasurface based on graphene strips

The proposed structure is shown in Fig. 1, which can exhibit the cloaking behaviour. In this model, a dielectric cylinder under illumination of *TE* and *TM* polarized plane waves is used. The z component of electric and magnetic fields for *TM* and *TE* polarizations can be written in terms of Bessel and Hankel functions as follows, respectively [78]:

$$E_i = \hat{z}\, E_0 \sum_{n=-\infty}^{\infty} j^{-n} J_n(\beta_0 r)\, e^{jn\phi} \tag{1}$$

Optics EXPRESS

$$E_s = \hat{z}\, E_0 \sum_{n=-\infty}^{\infty} j^{-n}\, c_{n(TM)}\, H_n^{(2)}(\beta_0 r)\, e^{jn\phi} \tag{2}$$

$$E_{in} = \hat{z}\, E_0 \sum_{n=-\infty}^{\infty} j^{-n}\, a_{n(TM)}\, J_n(\beta r)\, e^{jn\phi} \tag{3}$$

$$H_i = \hat{z}\, E_0 \sum_{n=-\infty}^{\infty} j^{-n} J_n(\beta_0 r)\, e^{jn\phi} \tag{4}$$

$$H_s = \hat{z}\, E_0 \sum_{n=-\infty}^{\infty} j^{-n}\, c_{n(TE)}\, H_n^{(2)}(\beta_0 r)\, e^{jn\phi} \tag{5}$$

$$H_{in} = \hat{z}\, E_0 \sum_{n=-\infty}^{\infty} j^{-n}\, a_{n(TE)}\, J_n(\beta r)\, e^{jn\phi} \tag{6}$$

where J_n and $H_n^{(2)}$ are Bessel function of the first type and Hankel function of the second type, respectively. β_0 and β are propagation constants in the air (here considered as the background medium) and in the cylinder with defined relative permittivity. Subscripts i, s and in represent incident field, scattered field and the field inside the object, respectively.

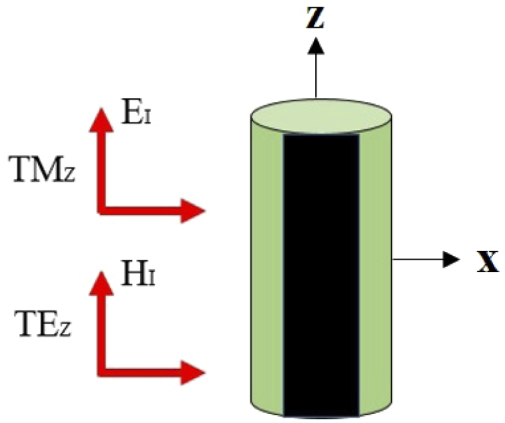

Fig. 1. Dielectric cylinder under TE and TM polarized incident waves.

Applying boundary conditions of continuity of tangential electric field and discontinuity of magnetic field as a result of introducing the covering metasurface, and by considering the following relations:

$$H_{\phi(TM)} = \frac{1}{jw\mu} \frac{\partial E_{z(TM)}}{\partial r} \tag{7}$$

$$E_{\phi(TE)} = -\frac{1}{jw\epsilon} \frac{\partial H_{z(TE)}}{\partial r} \tag{8}$$

one can achieve scattering coefficients for the two polarizations. By equating the scattering coefficients to zero, the required surface impedances for the both polarizations are obtained.

Monti et al. [76], demonstrated that the required surface impedance to achieve cloaking is different for *TE* and *TM* polarizations and invisibility can not be achieved for the two polarizations simultaneously at the same centre frequency with an isotropic metasurface. Therefore, an anisotropic metasurface should be designed whose surface impedance is set in each direction,

Optics EXPRESS

independently. Graphene strips as the covering metasurface are considered for this purpose. The proposed structure is shown in Fig. 2. For the planar configuration it exhibits a surface impedance tensor as follows [79]:

$$z_{zz} = z_s \frac{p}{a} \tag{9}$$

$$z_{xx} = z_s \frac{a}{p} + \frac{g}{p\,\sigma_c} \tag{10}$$

$$\sigma_c = \frac{j\omega\epsilon_0 p}{\pi} \ln \csc(\frac{\pi g}{2p}) \tag{11}$$

where p and a are periodicity and size of the strips, respectively, $g = p - a$ is the gap distance between two strips and z_s is the surface impedance of graphene. Surface conductivity of graphene which is revers of surface impedance is modeled by Kubo formula [80,81]. It is the sum of *intra* and *inter* conductivity:

$$\sigma_{intra} = -j\frac{K_B e^2 T}{\pi\hbar^2(w - 2j\tau^{-1})}[\frac{\mu_c}{K_B T} + 2\ln(e^{-\frac{\mu_c}{K_B T}} + 1)] \tag{12}$$

$$\sigma_{inter} = \frac{je^2}{4\pi\hbar} \ln\left(\frac{2|\mu_c| - (w - j\tau^{-1})\hbar}{2|\mu_c| + (w - j\tau^{-1})\hbar}\right) \tag{13}$$

where K_B is Boltzmann's constant, e is the electron charge, μ_c is the chemical potential, τ is the relaxation time, T is the temperature and $\hbar$ is the reduced Plank′s constant. The chemical potential of graphene can be adjusted by applying different bias voltages resulting in different surface impedances.

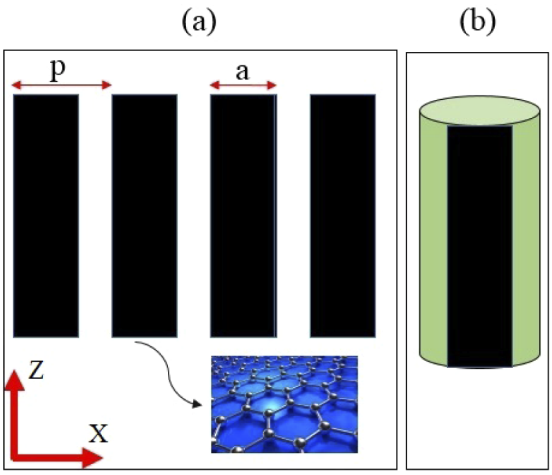

Fig. 2. (a) Structure of graphene strips, (b) A dielectric cylinder coated by graphene strips.

To design the proposed metasurface the following steps have been followed:

1. Obtaining the required surface impedance of the metasurface (z_{zz}) for achieving invisibility for TM_z polarization, using the formula (14) from [23] which is useful for infinite cylinder:

$$z_{zz} = \frac{2}{\omega a_1 \epsilon_0(\epsilon_r - 1)} \tag{14}$$

where a_1 and ϵ_r are radius and relative permittivity of the cylinder.

Optics EXPRESS

2. Obtaining the required surface impedance of the metasurface for *TE* polarization invisibility (z_{xx}). There is no closed form expression for cloaking a cylinder under illumination of *TE* polarization [76]. The required surface impedance can be achieved by optimization.
3. Choosing the characteristics of graphene and obtaining its surface impedance (z_s).
4. Achieving the ratio of p/a using eq. (9).
5. By knowing the ratio of g/p from p/a, σ_c is achieved using eq. (10).
6. The periodicity of the strips (p) will be obtained by eq. (11) and by knowing the ratio of p/a, the width of srtips (a) is also obtained. For give more insight about the design of metasurface, its pseudo code of metasurface design is reported in the following:

Algorithm 1: Metasurface design

function Metasurface $(\epsilon_r, a_1, \omega_1, \mu_c, T)$;
  $Z_{zz} :\leftarrow (\epsilon_r, a_1, \omega_1)$
  $Z_{xx} :\leftarrow (\epsilon_r, a_1, \omega_1)$
if $\mu_c \neq 0$ **then**
  $Z_s \leftarrow \sigma_{intra}, \sigma_{inter}$, T, μ_c ;
  calculation of p/a; from Z_s and Z_{zz};
  calculation of σ_c; from Z_{xx};
  calculation of p ; from σ_c
else
  return Metasurface$(\epsilon_1, \epsilon_r, a_1, \omega_1, \mu_c, T)$;
end

3. Results and discussions

To benchmark the performance of the proposed metasurface model, a numerical method is employed to simulate the structure. To sense of terahertz frequencies, the RCS spectra of the structure in regimes of cloaking and uncloaking is calculated. Here we aim to cloak a dielectric cylinder with radius of $a_1 = 10\mu$m and relative permittivity of $\epsilon_r = 4$ for *TE* and *TM* polarizations at a reference frequency of $f_r = 2.5$THz. The required surface reactance to achieve invisibility for *TE* and *TM* polarizations are obtained as: 234Ω and 404Ω, respectively. We choose the characteristic of graphene as: $\mu_c = 0.4$eV, $\tau = 1$ps and $T = 300$K resulting in $z_s = j333.7\Omega$. Following the procedure in the previous section we obtain $a = 19.2\mu$m and $p = 24\mu$m. It is worth noting that because the number of strips covering the cylinder should be integer and the obtained periodicity and size of the stirps lead to a non integer number of strips, optimization is needed. The optimized values for z_{xx} and z_{zz} is illustrated in Fig. 3 which at 2.5THz are very close to ones which have been achieved analytically. It can be seen that the required surface impedance for TM polarization shown by a green dot is very close to the surface impedance of the metasurface in the z axis. However, the required surface impedance for TE polarization shown by a blue star has a small difference with the surface impedance of the metasurface. The reason is that the surface impedance tensor has been derived for a planer structure while in this research, it has been used for bending structure. This can have low impact on z direction but more impact on x direction. The result is that for TE polarization, more optimization is needed.

Figure 4 shows RCS of uncloaked and cloaked cylinders for *TM* and *TE* polarizations illustrating simultaneous scattering reduction at 2.5THz for the two considered polarizations. It can also be seen that scattering reduction for *TM* polarization is much higher than that of *TE* polarization. We

Optics EXPRESS

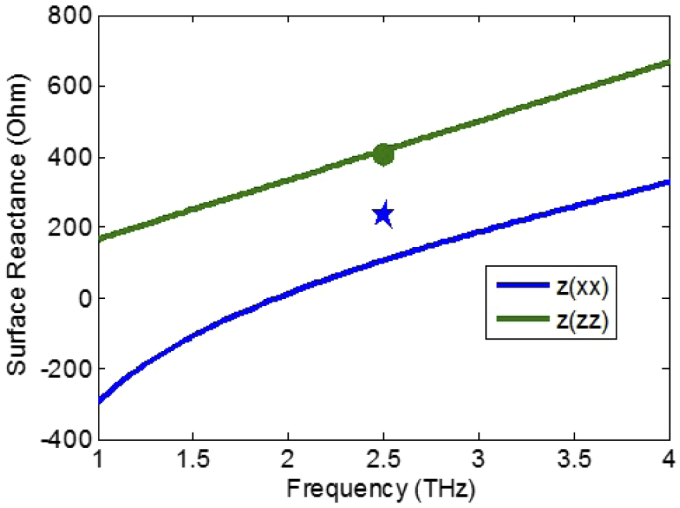

Fig. 3. The surface impedance tensor elements z_{xx} and z_{zz} for the optimized parameters of the proposed structure. The determined points with a star and dot correspond to the required surface impedances for z_{xx} and z_{zz}, respectively.

refer to [75] which provides an explanation for the reason of this difference. It is illustrated that for *TM* polarization, the scattering related to the first harmonic is more pronounced than the other harmonics and by canceling the scattering of the first harmonic, significant RCS reduction can be achieved. However for *TE* polarization, the first three harmonics have very similar amplitude and by canceling one harmonic, the other harmonics still play their role in the scattered field.

Effect of the relaxation time of graphene on the cloaking performance has been studied. Figure 5 shows the RCS of the cloaked cylinder for different relaxation times of graphene for *TE* and *TM* polarizations. It reveals that higher relaxation time results in better cloaking performance and lower RCS of the cylinder for both polarizations. The reason is that higher relaxation time leads to lower loss of graphene.

We exploit the extraordinary property of graphene to achieve tunable invisibility by changing chemical potential of graphene. Figures 6(a) and 6(b) show RCS of the cloaked cylinder with graphene strips for different chemical potentials. The figure indicates a shift in frequency of cloaking to 2.1THz and 2.8THz with chemical potential of 0.25eV and 0.55eV, respectively.

Distribution of the electric field related to *TE* and *TM* polarizations for uncloaked and cloaked cylinders is shown in Fig. 7 which depicts that covering the cylinder by the designed graphene strips reduces scattering for both polarizations so that the incident plane waves pass the object with a small perturbation. Figure 8 shows distribution of the electric field at 2.1THz and 2.8THz for cloaked cylinders under illumination of *TE* and *TM* polarizations. It indicates that the incident waves can be considered as plane waves after passing the cylinders which means the scattering from the cylinders can be neglected at these frequencies.

Numerical results obtained by two commercial software CST Microwave Studio and HFSS confirm RCS reduction for *TM* polarization in $\phi = 0^\circ$ plane and for *TE* polarization in plane $\theta = 0^\circ$ in polar system are shown in Fig. 9. Furthermore, the results from the two software show good agreement.

The designed graphene strips can operate as a covering metasurface for invisibility purpose also for circular polarization. This claim is proved in Fig. 10 which shows scattering reduction for circular polarization at 2.5THz.

Optics EXPRESS

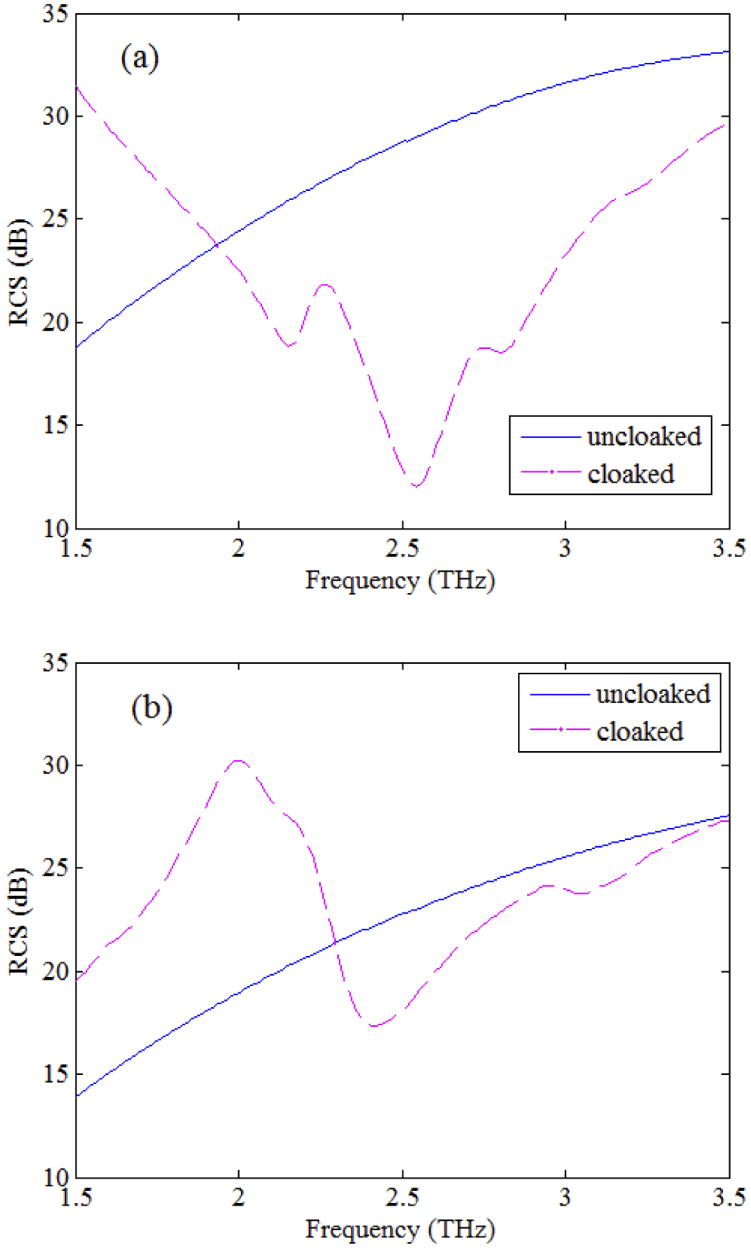

Fig. 4. RCS of uncloaked and cloaked cylinders with anisotropic metasurface for (a) *TM* polarized incident wave and (b) *TE* polarized incident wave.

Optics EXPRESS

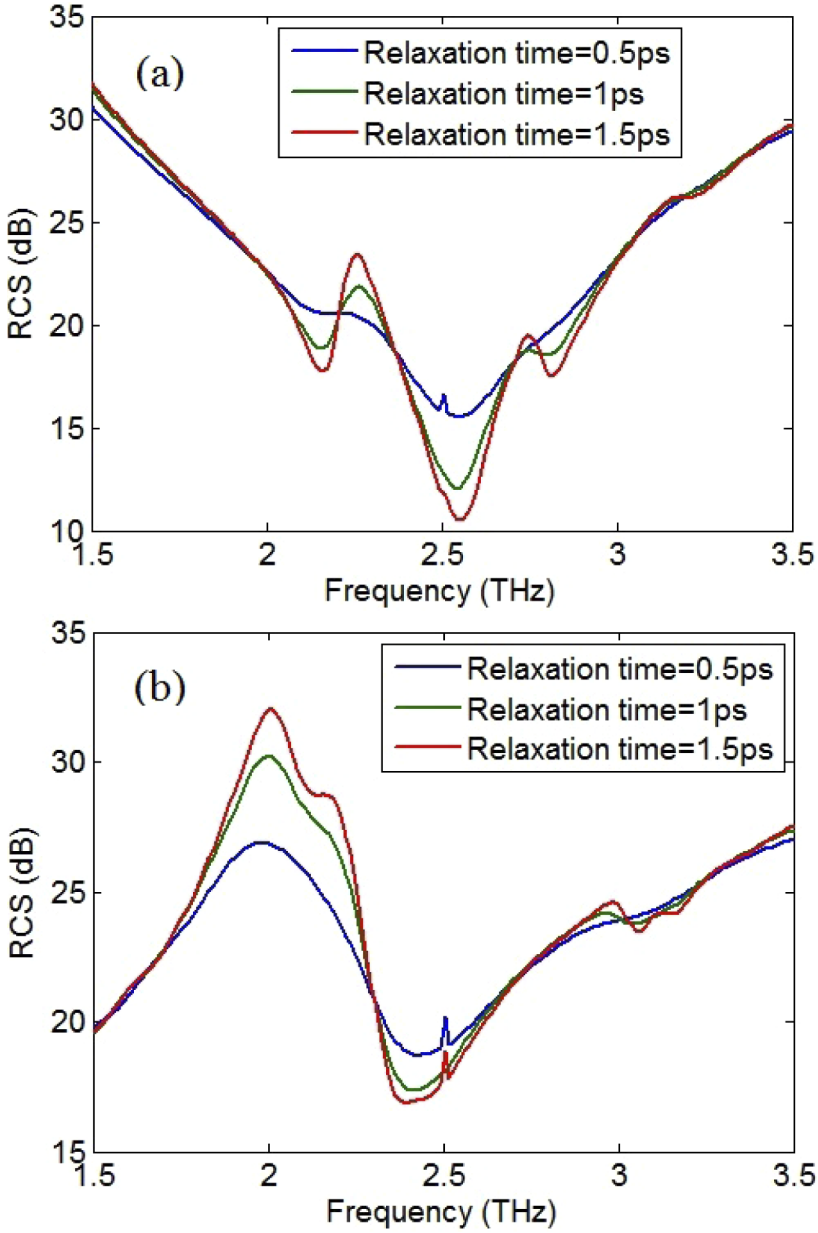

Fig. 5. RCS of the cloaked cylinders for different amounts of the relaxation time of graphene for (a) *TM*, (b) *TE* polarizations.

Optics EXPRESS

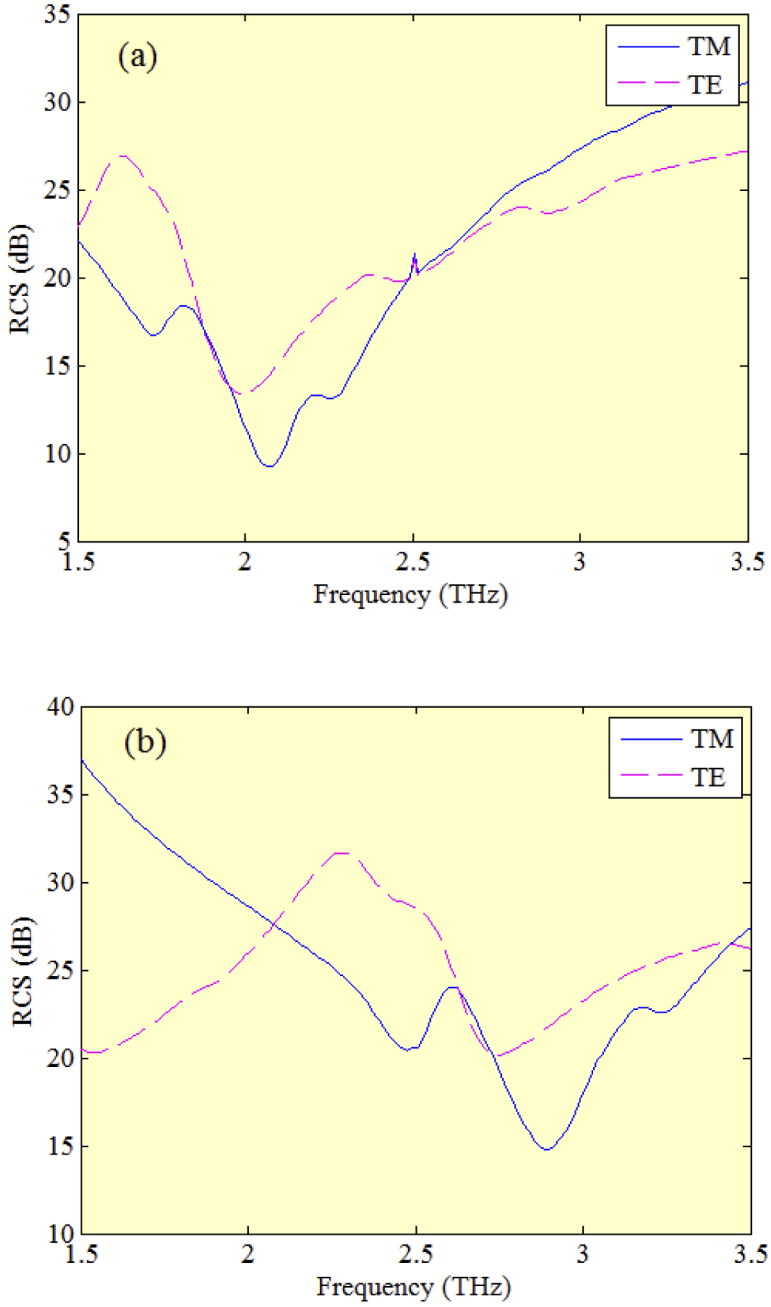

Fig. 6. RCS of uncloaked and cloaked cylinders with anisotropic metasurface for *TE* and *TM* polarizations with the chemical potential of (a) 0.25eV and (b) 0.55eV.

Optics EXPRESS

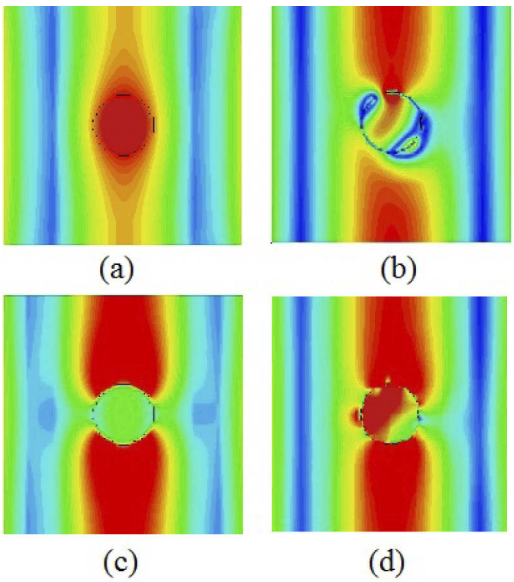

Fig. 7. Electric field distribution for the (a) uncloaked and (b) cloaked cylinders for *TM* polarization and (c) uncloaked and (d) cloaked cylinders for *TE* polarization

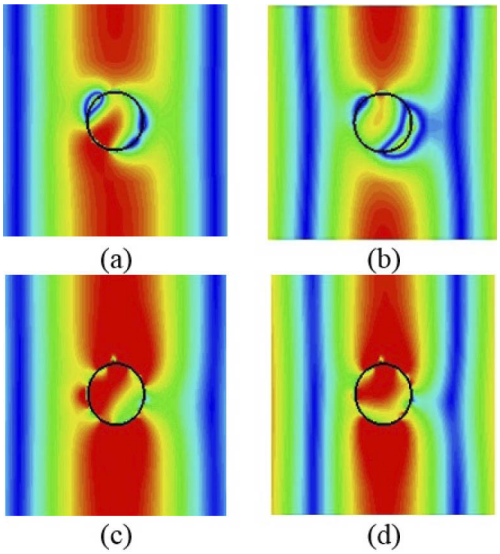

Fig. 8. Electric field distribution for the cloaked cylinders for (a) and (b) *TM* polarization, (c) and (d) *TE* polarization. (a) and (c) at 2.1THz, (b) and (d) at 2.8THz.

Optics EXPRESS

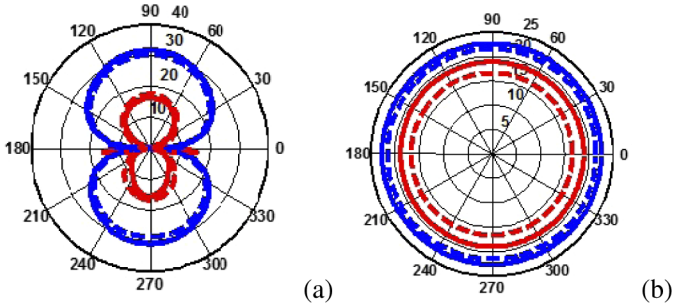

Fig. 9. Polar plot of RCS related to cloaked and uncloaked cylinders for (a) *TM* polarized incident wave in $\phi = 0°$ plane and for (b) *TE* polarized incident wave in $\theta = 0°$ plane. Blue: uncloaked, Red: cloaked, Dashed line: CST, Solid line: HFSS

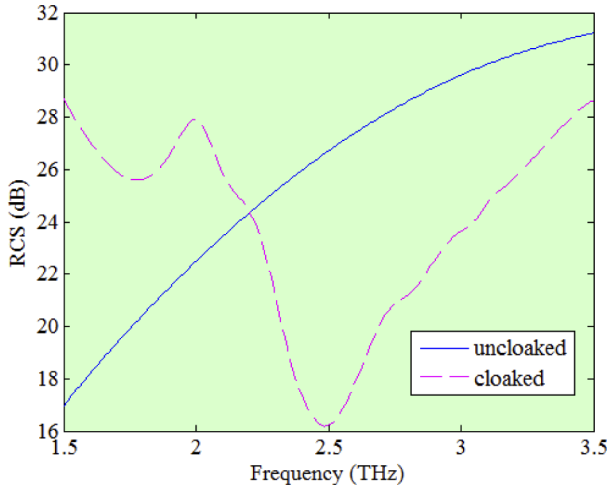

Fig. 10. RCS of cloaked and uncloaked cylinders under illumination of circular polarized waves.

4. Conclusion

A tunable mantle cloaking of a dielectric cylinder under *TE* and *TM* polarizations in terahertz range was proposed. By considering the tunable optical properties of graphene metasurface, tunable cloaking behaviour of the proposed structure was investigated. For this purpose, an anisotropic metasurface based on graphene strips has been considered. The proposed covering structure and characteristics of graphene have been designed so that the required surface impedance tensor for achieving invisibility for both polarizations has been obtained. Scattered wave from the cylinder under illumination of circularly polarized wave can also decreases with the designed metasurface. Furthermore, by properly changing the chemical potential of graphene, tunable mantle cloaking has been achieved. To evaluate of the structure and to obtain high reduction in scattering, the numerical software including CST Microwave Studio and HFSS were considered. Numerical results show 2-11 dB reduction in scattering strength relative to the uncloaked configuration for 0.3eV variation of graphene chemical potential. We believe that the proposed model can open up novel avenues for practical applications of high resolution cloaking sensors.

Optics EXPRESS

References

1. T. Yang, X. Bai, D. Gao, L. Wu, B. Li, J. T. Thong, and C.-W. Qiu, "Invisible sensors: simultaneous sensing and camouflaging in multiphysical fields," Adv. Mater. **27**(47), 7752–7758 (2015).
2. A. Alu and N. Engheta, "Cloaking a receiving antenna or a sensor with plasmonic metamaterials," Metamaterials **4**(2-3), 153–159 (2010).
3. A. Khademi, T. Dewolf, and R. Gordon, "Quantum plasmonic epsilon near zero: field enhancement and cloaking," Opt. Express **26**(12), 15656–15664 (2018).
4. M. D. Guild, A. Alu, and M. R. Haberman, "Cloaking of an acoustic sensor using scattering cancellation," Appl. Phys. Lett. **105**(2), 023510 (2014).
5. R. Fleury and A. Alu, "Cloaking and invisibility: A review," in *Forum for Electromagnetic Research Methods and Application Technologies (FERMAT)*, vol. 1 (2014).
6. G. Labate, S. K. Podilchak, and L. Matekovits, "Closed-form harmonic contrast control with surface impedance coatings for conductive objects," Appl. Opt. **56**(36), 10055–10059 (2017).
7. A. K. Ospanova, G. Labate, L. Matekovits, and A. A. Basharin, "Multipolar passive cloaking by nonradiating anapole excitation," Sci. Rep. **8**(1), 12514 (2018).
8. M. Selvanayagam and G. V. Eleftheriades, "An active electromagnetic cloak using the equivalence principle," IEEE Antennas Wirel. Propag. Lett. **11**, 1226–1229 (2012).
9. A. Rajput and K. V. Srivastava, "Dual-band cloak using microstrip patch with embedded u-shaped slot," IEEE Antennas Wirel. Propag. Lett. **16**, 2848–2851 (2017).
10. P. Vura, A. Rajput, and K. V. Srivastava, "Composite-shaped external cloaks with homogeneous material properties," IEEE Antennas Wirel. Propag. Lett. **15**, 282–285 (2016).
11. Y. Shi, W. Tang, L. Li, and C.-H. Liang, "Three-dimensional complementary invisibility cloak with arbitrary shapes," IEEE Antennas Wirel. Propag. Lett. **14**, 1550–1553 (2015).
12. Z. Hamzavi-Zarghani, A. Yahaghi, and A. Bordbar, "Analytical design of nanostructured graphene metasurface for controllable scattering manipulation of dielectric cylinder," in *Electrical Engineering (ICEE), Iranian Conference on*, (IEEE, 2018), pp. 592–595.
13. Z. Hamzavi-Zarghani, A. Yahaghi, and L. Matekovits, "Dynamically tunable scattering manipulation of dielectric and conducting cylinders using nanostructured graphene metasurfaces," IEEE Access **7**, 15556–15562 (2019).
14. J. B. Pendry, D. Schurig, and D. R. Smith, "Controlling electromagnetic fields," Science **312**(5781), 1780–1782 (2006).
15. D. Schurig, J. Mock, B. Justice, S. A. Cummer, J. B. Pendry, A. Starr, and D. Smith, "Metamaterial electromagnetic cloak at microwave frequencies," Science **314**(5801), 977–980 (2006).
16. A. Alu, D. Rainwater, and A. Kerkhoff, "Plasmonic cloaking of cylinders: finite length, oblique illumination and cross-polarization coupling," New J. Phys. **12**(10), 103028 (2010).
17. M. Danaeifar, N. Granpayeh, and M. R. Booket, "Optical invisibility of cylindrical structures and homogeneity effect on scattering cancellation method," Electron. Lett. **52**(1), 29–31 (2016).
18. M. Nisar and Q. A. Naqvi, "Cloaking and magnifying using radial anisotropy in non-integer dimensional space," Phys. Lett. A **382**(31), 2055–2060 (2018).
19. A. Darabi, A. Zareei, M.-R. Alam, and M. J. Leamy, "Experimental demonstration of an ultrabroadband nonlinear cloak for flexural waves," Phys. Rev. Lett. **121**(17), 174301 (2018).
20. A. Shahzad, S. Ahmed, A. Ghaffar, and Q. Naqvi, "Incorporation of the nihility medium to improve the cylindrical invisibility cloak," *ACES J.* 29(1), (2014).
21. M. Rajabi and A. Mojahed, "Active acoustic cloaking spherical shells," Acta Acust. Acust. **104**(1), 5–12 (2018).
22. A. Shahzad, F. Qasim, S. Ahmed, and Q. A. Naqvi, "Cylindrical invisibility cloak incorporating pemc at perturbed void region," Prog. Electromagn. Res. **21**, 61–76 (2011).
23. A. Alu, "Mantle cloak: Invisibility induced by a surface," Phys. Rev. B **80**(24), 245115 (2009).
24. G. Labate, A. Alu, and L. Matekovits, "Surface-admittance equivalence principle for nonradiating and cloaking problems," Phys. Rev. A **95**(6), 063841 (2017).
25. A. Forouzmand and A. B. Yakovlev, "Electromagnetic cloaking of a finite conducting wedge with a nanostructured graphene metasurface," IEEE Trans. Antennas Propag. **63**(5), 2191–2202 (2015).
26. P.-Y. Chen and A. Alu, "Atomically thin surface cloak using graphene monolayers," ACS Nano **5**(7), 5855–5863 (2011).
27. S. Vellucci, A. Monti, M. Barbuto, A. Toscano, and F. Bilotti, "Satellite applications of electromagnetic cloaking," IEEE Trans. Antennas Propag. **65**(9), 4931–4934 (2017).
28. H. Younesiraad, M. Bemani, and S. Nikmehr, "Scattering suppression and cloak for electrically large objects using cylindrical metasurface based on monolayer and multilayer mantle cloak approach," IET Microwaves, Antennas Propag. **13**(3), 278–285 (2019).
29. L. Matekovits and T. S. Bird, "Width-modulated microstrip-line based mantle cloaks for thin single-and multiple cylinders," IEEE Trans. Antennas Propag. **62**(5), 2606–2615 (2014).
30. T. V. Teperik, S. N. Burokur, A. de Lustrac, G. Sabanowski, and G.-P. Piau, "Experimental validation of an ultra-thin metasurface cloak for hiding a metallic obstacle from an antenna radiation at low frequencies," Appl. Phys. Lett. **111**(5), 054105 (2017).

Optics EXPRESS

31. M. Danaeifar and N. Granpayeh, "Wideband invisibility by using inhomogeneous metasurfaces of graphene nanodisks in the infrared regime," J. Opt. Soc. Am. B **33**(8), 1764–1768 (2016).
32. E. Shokati, N. Granpayeh, and M. Danaeifar, "Wideband and multi-frequency infrared cloaking of spherical objects by using the graphene-based metasurface," Appl. Opt. **56**(11), 3053–3058 (2017).
33. M. Qin, L. Wang, X. Zhai, and S. Xia, "Multispectral resonances and coherent control in plasmonic metasurfaces," IEEE Photonics Technol. Lett. **31**(4), 319–322 (2019).
34. M. Qin, L. Wang, X. Zhai, Q. Lin, and S. Xia, "Multispectral plasmon induced transparency in a defective metasurface plasmonic nanostructure," IEEE Photonics Technol. Lett. **30**(11), 1009–1012 (2018).
35. G.-D. Liu, X. Zhai, S.-X. Xia, Q. Lin, C.-J. Zhao, and L.-L. Wang, "Toroidal resonance based optical modulator employing hybrid graphene-dielectric metasurface," Opt. Express **25**(21), 26045–26054 (2017).
36. M. Baqir, A. Farmani, T. Fatima, M. Raza, S. Shaukat, and A. Mir, "Nanoscale, tunable, and highly sensitive biosensor utilizing hyperbolic metamaterials in the near-infrared range," Appl. Opt. **57**(31), 9447–9454 (2018).
37. S. Khani, M. Danaie, and P. Rezaei, "Tunable single-mode bandpass filter based on metal–insulator–metal plasmonic coupled u-shaped cavities," IET Optoelectron. **13**(4), 161–171 (2019).
38. A. Farmani, A. Mir, M. Bazgir, and F. B. Zarrabi, "Highly sensitive nano-scale plasmonic biosensor utilizing fano resonance metasurface in thz range: numerical study," Phys. E (Amsterdam, Neth.) **104**, 233–240 (2018).
39. A. Alipour, A. Farmani, and A. Mir, "High sensitivity and tunable nanoscale sensor based on plasmon-induced transparency in plasmonic metasurface," IEEE Sens. J. **18**(17), 7047–7054 (2018).
40. M. Hosseinifar, V. Ahmadi, and M. Ebnali-Heidari, "Schottky graphene/si photodetector based on metal-dielectric hybrid hollow-core photonic crystal fibers," Opt. Lett. **42**(24), 5066–5069 (2017).
41. A. Farmani and A. Mir, "Graphene sensor based on surface plasmon resonance for optical scanning," IEEE Photonics Technol. Lett. **31**(8), 643–646 (2019).
42. Z. Vafapour, Y. Hajati, M. Hajati, and H. Ghahraloud, "Graphene-based mid-infrared biosensor," J. Opt. Soc. Am. B **34**(12), 2586–2592 (2017).
43. A. Farmani, "Three-dimensional fdtd analysis of a nanostructured plasmonic sensor in the near-infrared range," J. Opt. Soc. Am. B **36**(2), 401–407 (2019).
44. M. Janfaza, M. A. Mansouri-Birjandi, and A. Tavousi, "Proposal for a graphene nanoribbon assisted mid-infrared band-stop/band-pass filter based on bragg gratings," Opt. Commun. **440**, 75–82 (2019).
45. A. Farmani, M. Miri, and M. H. Sheikhi, "Tunable resonant goos–hänchen and imbert–fedorov shifts in total reflection of terahertz beams from graphene plasmonic metasurfaces," J. Opt. Soc. Am. B **34**(6), 1097–1106 (2017).
46. M. Dehghan, M. K. Moravvej-Farshi, M. Ghaffari-Miab, M. Jabbari, and G. Darvish, "Ultra-compact spatial terahertz switch based on graphene plasmonic-coupled waveguide," *Plasmonics* 1–11 (2019).
47. S. Xiao, T. Liu, L. Cheng, C. Zhou, X. Jiang, Z. Li, and C. Xu, "Tunable anisotropic absorption in hyperbolic metamaterials based on black phosphorous/dielectric multilayer structures," J. Lightwave Technol. **37**(13), 3290–3297 (2019).
48. P.-Y. Chen, J. Soric, Y. R. Padooru, H. M. Bernety, A. B. Yakovlev, and A. Alu, "Nanostructured graphene metasurface for tunable terahertz cloaking," New J. Phys. **15**(12), 123029 (2013).
49. T. Liu, C. Zhou, L. Cheng, X. Jiang, G. Wang, C. Xu, and S. Xiao, "Actively tunable slow light in a terahertz hybrid metal-graphene metamaterial," J. Opt. **21**(3), 035101 (2019).
50. X. Wang, G. Liu, S. Xia, H. Meng, X. Shang, P. He, and X. Zhai, "Dynamically tunable fano resonance based on graphene metamaterials," IEEE Photonics Technol. Lett. **30**(24), 2147–2150 (2018).
51. T. Liu, H. Wang, Y. Liu, L. Xiao, Z. Yi, C. Zhou, and S. Xiao, "Active manipulation of electromagnetically induced transparency in a terahertz hybrid metamaterial," Opt. Commun. **426**, 629–634 (2018).
52. Y. Fan, N.-H. Shen, F. Zhang, Q. Zhao, H. Wu, Q. Fu, Z. Wei, H. Li, and C. M. Soukoulis, "Graphene plasmonics: A platform for 2d optics," Adv. Opt. Mater. **7**(3), 1800537 (2019).
53. M. Rahmanshahi, S. Golmohammadi, H. Baghban, and A. Asgari, "Photonics Nanostructures-Fundamentals Appl.," Photonics Nanostructures-Fundamentals Appl. **31**, 173–179 (2018).
54. V. K. Sadaghiani, M. Zavvari, M. B. Tavakkoli, and A. Horri, "Design of graphene-based hybrid waveguides for nonlinear applications," Opt. Quantum Electron. **51**(2), 49 (2019).
55. M. M. Mehrnegar, S. Darbari, H. Ramezani, and M. K. Moravvej-Farshi, "Designing graphene-based multi-mode acousto-plasmonic devices," J. Lightwave Technol. **37**(9), 2126–2132 (2019).
56. S. Asgari, N. Granpayeh, and Z. G. Kashani, "Plasmonic mid-infrared wavelength selector and linear logic gates based on graphene cylindrical resonator," IEEE Trans. Nanotechnol. **18**, 42–50 (2019).
57. M. H. Rezaei, A. Zarifkar, and M. Miri, "Ultra-compact electro-optical graphene-based plasmonic multi-logic gate with high extinction ratio," Opt. Mater. **84**, 572–578 (2018).
58. A. Farmani, A. Mir, and Z. Sharifpour, "Broadly tunable and bidirectional terahertz graphene plasmonic switch based on enhanced goos-hanchen effect," Appl. Surf. Sci. **453**, 358–364 (2018).
59. Z. Hamzavi-Zarghani, A. Yahaghi, and L. Matekovits, "Tunable lens based on graphene metasurface for circular polarization," in *2018 International Conference on Electromagnetics in Advanced Applications (ICEAA)*, (IEEE, 2018), pp. 644–647.
60. Z. Hamzavi-Zarghani, A. Yahaghi, and L. Matekovits, "Reconfigurable metasurface lens based on graphene split ring resonators using pancharatnam–berry phase manipulation," J. Electromagn. Waves Appl. **33**(5), 572–583 (2019).

Optics EXPRESS

61. Z. Hamzavi-Zarghani, A. Yahaghi, L. Matekovits, and I. Peter, "Tunable polarization converter based on graphene metasurfaces," in *2018 IEEE Radio and Antenna Days of the Indian Ocean (RADIO)*, (IEEE, 2018), pp. 1–2.
62. A. Farmani, M. Miri, and M. H. Sheikhi, "Design of a high extinction ratio tunable graphene on white graphene polarizer," IEEE Photonics Technol. Lett. **30**(2), 153–156 (2018).
63. E. S. Torabi, A. Fallahi, and A. Yahaghi, "Evolutionary optimization of graphene-metal metasurfaces for tunable broadband terahertz absorption," IEEE Trans. Antennas Propag. **65**(3), 1464–1467 (2017).
64. S. K. Ghosh, V. S. Yadav, S. Das, and S. Bhattacharyya, "Tunable graphene-based metasurface for polarization-independent broadband absorption in lower mid-infrared (mir) range," IEEE Trans. Electromagn. Compat. 1–9 (2019).
65. S.-X. Xia, X. Zhai, Y. Huang, J.-Q. Liu, L.-L. Wang, and S.-C. Wen, "Graphene surface plasmons with dielectric metasurfaces," J. Lightwave Technol. **35**(20), 4553–4558 (2017).
66. S. Das, P. Sudhagar, V. Verma, D. Song, E. Ito, S. Y. Lee, Y. S. Kang, and W. Choi, "Amplifying charge-transfer characteristics of graphene for triiodide reduction in dye-sensitized solar cells," Adv. Funct. Mater. **21**(19), 3729–3736 (2011).
67. X. Huang, X. Zhang, Z. Hu, M. Aqeeli, and A. Alburaikan, "Design of broadband and tunable terahertz absorbers based on graphene metasurface: equivalent circuit model approach," IET Microwaves, Antennas Propag. **9**(4), 307–312 (2015).
68. R. Ning, Z. Jiao, and J. Bao, "Multi-band and wide-band electromagnetically induced transparency in graphene metasurface of composite structure," IET Microwaves, Antennas Propag. **12**(3), 380–384 (2018).
69. V. S. Yadav, S. K. Ghosh, S. Bhattacharyya, and S. Das, "Graphene-based metasurface for a tunable broadband terahertz cross-polarization converter over a wide angle of incidence," Appl. Opt. **57**(29), 8720–8726 (2018).
70. B. Zhu, G. Ren, S. Zheng, Z. Lin, and S. Jian, "Nanoscale dielectric-graphene-dielectric tunable infrared waveguide with ultrahigh refractive indices," Opt. Express **21**(14), 17089–17096 (2013).
71. M. Grande, G. V. Bianco, D. Laneve, P. Capezzuto, V. Petruzzelli, M. Scalora, F. Prudenzano, G. Bruno, and A. D'Orazio, "Gain and phase control in a graphene-loaded reconfigurable antenna," Appl. Phys. Lett. **115**(13), 133103 (2019).
72. Z. Hamzavi-Zarghani, A. Yahaghi, and L. Matekovits, "Analytical design of a metasurface based mantle cloak for dielectric cylinder under oblique incidence," in *2018 9th International Symposium on Telecommunications (IST)*, (IEEE, 2018), pp. 65–68.
73. Y. R. Padooru, A. B. Yakovlev, C. S. Kaipa, G. W. Hanson, F. Medina, and F. Mesa, "Dual capacitive-inductive nature of periodic graphene patches: Transmission characteristics at low-terahertz frequencies," Phys. Rev. B **87**(11), 115401 (2013).
74. R. Emadi, R. Safian, A. Z. Nezhad, and N. Barani, "Robust multi-layer graphene-based plasmonic cloaking," in *2018 USNC-URSI Radio Science Meeting (Joint with AP-S Symposium)*, (IEEE, 2018), pp. 145–146.
75. J. Soric, P. Chen, A. Kerkhoff, D. Rainwater, K. Melin, and A. Alù, "Demonstration of an ultralow profile cloak for scattering suppression of a finite-length rod in free space," New J. Phys. **15**(3), 033037 (2013).
76. A. Monti, J. C. Soric, A. Alù, A. Toscano, and F. Bilotti, "Anisotropic mantle cloaks for tm and te scattering reduction," IEEE Trans. Antennas Propag. **63**(4), 1775–1788 (2015).
77. J. S. Gomez-Diaz, M. Tymchenko, and A. Alu, "Hyperbolic plasmons and topological transitions over uniaxial metasurfaces," Phys. Rev. Lett. **114**(23), 233901 (2015).
78. C. A. Balanis, *Advanced engineering electromagnetics* (John Wiley and Sons, 1999).
79. S. A. H. Gangaraj, T. Low, A. Nemilentsau, and G. W. Hanson, "Directive surface plasmons on tunable two-dimensional hyperbolic metasurfaces and black phosphorus: Green's function and complex plane analysis," IEEE Trans. Antennas Propag. **65**(3), 1174–1186 (2017).
80. G. W. Hanson, "Erratum:"dyadic green's functions and guided surface waves for a surface conductivity model of graphene" [j. appl. phys. 103, 064302 (2008)]," J. Appl. Phys. **113**(2), 029902 (2013).
81. M. Biabanifard and M. S. Abrishamian, "Multi-band circuit model of tunable thz absorber based on graphene sheet and ribbons," AEU-International J. Electron. Commun. **95**, 256–263 (2018).